Space-Mapping Optimization of Microwave Circuits Exploiting Surrogate Models

Mohamed H. Bakr, *Student Member, IEEE,* John W. Bandler, *Fellow, IEEE,* Kaj Madsen, José Ernesto Rayas-Sánchez, *Senior Member, IEEE,* and Jacob Søndergaard

***Abstract*—A powerful new space-mapping (SM) optimization algorithm is presented in this paper. It draws upon recent developments in both surrogate model-based optimization and modeling of microwave devices. SM optimization is formulated as a general optimization problem of a surrogate model. This model is a convex combination of a mapped coarse model and a linearized fine model. It exploits, in a novel way, a linear frequency-sensitive mapping. During the optimization iterates, the coarse and fine models are simulated at different sets of frequencies. This approach is shown to be especially powerful if a significant response shift exists. The algorithm is illustrated through the design of a capacitively loaded 10 : 1 impedance transformer and a double-folded stub filter. A high-temperature superconducting filter is also designed using decoupled frequency and SMs.**

***Index Terms*—Design automation, EM optimization, microwave circuits, microstrip filters, optimization methods, space mapping, superconducting filters, surrogate models.**

I. Introduction

In THIS paper, we present a novel space mapping (SM) algorithm for microwave circuit optimization [1]. It integrates, for the first time, two distinct optimization approaches: SM optimization [2]–[4] and surrogate model-based optimization [5]–[7]. Both approaches aim at efficiently optimizing an accurate and time-intensive "fine" model, e.g., a full-wave electromagnetic (EM) simulator. SM exploits the existence of a less accurate, but fast "coarse" model. It formulates the design problem as a system of nonlinear equations. On the other hand, surrogate-based optimization, new to the microwave arena, exploits an approximate model in iteratively solving the original design problem. This model may be a less accurate physically based model or algebraic model [6].

Manuscript received February 27, 2000; revised August 21, 2000. This work was supported in part by the Natural Sciences and Engineering Research Council of Canada under Grant OGP0007239 and Grant STP0201832 and by the Micronet Network of Centres of Excellence. The work of M. H. Bakr was supported under an Ontario Graduate Scholarship. The work of J. E. Rayas-Sánchez was supported by the Consejo Nacional de Ciencia y Tecnología and by the Instituto Tecnológico y de Estudios Superiores de Occidente.

M. H. Bakr and J. E. Rayas-Sánchez are with the Simulation Optimization Systems Research Laboratory and the Department of Electrical and Computer Engineering, McMaster University, Hamilton, ON, Canada L8S 4K1.

J. W. Bandler is with the Simulation Optimization Systems Research Laboratory and the Department of Electrical and Computer Engineering, McMaster University, Hamilton, ON, Canada L8S 4K1 and also with the Bandler Corporation, Dundas, ON, Canada L9H 5E7.

K. Madsen and J. Søndergaard are with the Department of Mathematical Modeling, Technical University of Denmark, DK-2800 Lyngby, Denmark.

Publisher Item Identifier S 0018-9480(00)10723-9.

Our algorithm combines both approaches. The original design problem is iteratively solved using a surrogate model. This model is a convex combination of a mapped coarse model (MCM) and a linearized fine model (LFM). The accuracy of the surrogate model is improved in every iteration using the generated fine-model simulations.

Recent developments in space mapping-based neuromodeling (SMN) [8] and generalized space-mapping (GSM) modeling [9] exploit frequency-sensitive mappings. This approach is reported to improve the accuracy of SM-based models. We integrate this concept, in a novel way, with SM optimization. In each iteration, a linear frequency-sensitive mapping is exploited in constructing the MCM. Here, the coarse and fine models are simulated over different frequency ranges. This approach efficiently handles significant frequency shifts.

The established frequency-sensitive mapping obtains an estimate of the derivatives of the mapped coarse-model responses. These derivatives are expressed in terms of the coarse-model derivatives and mapping parameters. We show that this expression is a generalized form for frequency-sensitive mappings of the lemma utilized in [4]. It can be used to approximate the fine-model derivatives in the region of interest.

A number of examples are successfully solved. They include a capacitively loaded two-section 10 : 1 impedance transformer [10], a double-folded stub (DFS) filter [11] and a high-temperature superconducting (HTS) filter [12]. Decoupled frequency and SMs are utilized in the optimization of the HTS filter. This approach shows the feasibility of utilizing different types of frequency-sensitive mappings in the optimization loop.

II. SM Optimization Versus Surrogate-Based Optimization

We denote the fine-model responses at a point $\boldsymbol{x}_f \in \Re^{n\times 1}$ and frequency ω by $\boldsymbol{R}_f(\boldsymbol{x}_f, \omega) \in \Re^{N_r\times 1}$. These responses may include the real and imaginary parts of S_{11}, etc. The vector $\boldsymbol{R}_f(\boldsymbol{x}_f) \in \Re^{m\times 1}$ denotes the responses at all the N_ω simulation frequencies where $m = N_r N_\omega$. The original design problem is

$$\boldsymbol{x}_f^* = \arg\left\{\min_{\boldsymbol{x}_f} U(\boldsymbol{R}_f(\boldsymbol{x}_f))\right\} \tag{1}$$

where U is the objective function and $\boldsymbol{x}_f^*$ is the optimal fine-model design. Solving (1) using direct optimization methods, e.g., [13], is prohibitive due to the intensive simulation time of the fine model.

SM optimization exploits the existence of a fast, but less accurate, "coarse" model of the circuit. We denote by

$\boldsymbol{x}_c \in \Re^{n\times 1}$ and $\boldsymbol{R}_c(\boldsymbol{x}_c) \in \Re^{m\times 1}$ a coarse-model point and the corresponding coarse-model response vector, respectively. The coarse-model responses at a frequency ω_c are similarly denoted by $\boldsymbol{R}_c(\boldsymbol{x}_c, \omega_c) \in \Re^{N_r\times 1}$.

The first step in all SM-based optimization algorithms obtains the optimal coarse-model design $\boldsymbol{x}_c^*$. The corresponding response is denoted by $\boldsymbol{R}_c^* \in \Re^{m\times 1}$. SM aims at establishing a mapping $\boldsymbol{P}$ between the two spaces [2]

$$\boldsymbol{x}_c = \boldsymbol{P}(\boldsymbol{x}_f) \tag{2}$$

such that

$$\boldsymbol{R}_f(\boldsymbol{x}_f) \approx \boldsymbol{R}_c(\boldsymbol{x}_c) \tag{3}$$

over a region in the parameter space. SM optimization obtains a space-mapped design $\bar{\boldsymbol{x}}_f$ whose response matches $\boldsymbol{R}_c^*$. $\bar{\boldsymbol{x}}_f$ is a solution of the nonlinear system

$$\boldsymbol{f}(\boldsymbol{x}_f) = \boldsymbol{P}(\boldsymbol{x}_f) - \boldsymbol{x}_c^* = \boldsymbol{0} \tag{4}$$

where $\boldsymbol{P}(\boldsymbol{x}_f)$ is approximated through a parameter-extraction (PE) procedure.

Previous SM optimization algorithms [2]–[4] solve (4) iteratively. Let $\boldsymbol{x}_f^{(i)}$ be the ith iterate. Aggressive space mapping (ASM) [2] predicts a new iterate $\boldsymbol{x}_f^{(i+1)} = \boldsymbol{x}_f^{(i)} + \boldsymbol{h}^{(i)}$ by utilizing the quasi-Newton iteration

$$\boldsymbol{B}^{(i)}\boldsymbol{h}^{(i)} = -\boldsymbol{f}\left(\boldsymbol{x}_f^{(i)}\right). \tag{5}$$

$\boldsymbol{B}^{(i)}$ is an approximation to the Jacobian of $\boldsymbol{f}$ with respect to $\boldsymbol{x}_f$ at $\boldsymbol{x}_f^{(i)}$. It is updated at the end of every iteration using Broyden's update [14].

The trust region aggressive space mapping (TRASM) algorithm [3] minimizes $\|\boldsymbol{f}(\boldsymbol{x}_f^{(i+1)})\|$ using least squares within a trust region. The ith iteration of the algorithm is given by

$$\left(\boldsymbol{B}^{(i)T}\boldsymbol{B}^{(i)} + \psi\boldsymbol{I}\right)\boldsymbol{h}^{(i)} = -\boldsymbol{B}^{(i)T}\boldsymbol{f}^{(i)}. \tag{6}$$

Parameter ψ is selected such that $\|\boldsymbol{h}^{(i)}\| \le \delta^{(i)}$, where $\delta^{(i)}$ is the size of the trust region. The new iterates are accepted only if they are descent directions for $\|\boldsymbol{f}\|$. TRASM also utilizes a recursive multipoint extraction procedure to enhance the uniqueness of PE.

Hybrid aggressive space mapping (HASM) [4] addresses the problem of a poor coarse model. It adopts a two-phase approach. The first phase exploits a TRASM strategy. The second phase minimizes $\|\boldsymbol{R}_f(\boldsymbol{x}_f) - \boldsymbol{R}_c^*\|_2$ through direct least-squares optimization. A relationship relates the available mapping to the first-order derivatives of the responses of both models [4]. It is used for switching between the two phases.

Alternatively, an expensive model can be optimized indirectly by using a surrogate model [5]–[7]. This surrogate model may be a less accurate physics-based model or a polynomial approximation of the fine model [6]. We denote the surrogate model in the ith iteration by $\boldsymbol{R}_s^{(i)}(\boldsymbol{x}_f) \in \Re^{m\times 1}$. The ith iteration step is obtained by solving

$$\boldsymbol{h}^{(i)} = \arg\left\{\min_{\boldsymbol{h}^{(i)}} U\left(\boldsymbol{R}_s^{(i)}\left(\boldsymbol{x}_f^{(i)} + \boldsymbol{h}^{(i)}\right)\right)\right\}, \qquad \left\|\boldsymbol{h}^{(i)}\right\| \le \delta^{(i)} \tag{7}$$

where $U(\boldsymbol{R}_s^{(i)}(\boldsymbol{x}_f^{(i)} + \boldsymbol{h}^{(i)}))$ is the value of the objective function evaluated using the surrogate model at the point $\boldsymbol{x}_f^{(i)} + \boldsymbol{h}^{(i)}$. The point $\boldsymbol{x}_f^{(i)} + \boldsymbol{h}^{(i)}$ is then validated using fine-model simulation. It is accepted if it improves the fine-model objective function. Otherwise, the accuracy of $\boldsymbol{R}_s^{(i)}(\boldsymbol{x}_f)$ should be improved. Different strategies can be utilized for improving the surrogate model accuracy. One strategy utilizes only the validation fine-model simulations. Additional fine simulations may be generated to improve the surrogate model in certain directions of the parameter space.

III. Surrogate Model

In the ith iteration, our algorithm utilizes a surrogate model expressed as a convex combination of an LFM and an MCM $\boldsymbol{R}_m^{(i)}(\boldsymbol{x}_f)$. It is given by

$$\boldsymbol{R}_s^{(i)}(\boldsymbol{x}_f) = \lambda^{(i)}\boldsymbol{R}_m^{(i)}(\boldsymbol{x}_f) + \left(1-\lambda^{(i)}\right) \times \left(\boldsymbol{R}_f\left(\boldsymbol{x}_f^{(i)}\right) + \boldsymbol{J}_f^{(i)}\Delta\boldsymbol{x}_f\right), \qquad \lambda^{(i)} \in [0,1]. \tag{8}$$

$\boldsymbol{J}_f^{(i)} \in \Re^{m\times n}$ is an approximation to the Jacobian of fine-model responses at $\boldsymbol{x}_f^{(i)}$ and $\Delta\boldsymbol{x}_f = \boldsymbol{x}_f - \boldsymbol{x}_f^{(i)}$. The parameter $\lambda^{(i)}$ determines which model is favored. If $\lambda^{(i)} = 1$, the surrogate model becomes an MCM. If $\lambda^{(i)} = 0$, the surrogate model becomes an LFM. $\forall\lambda^{(i)} \in (0,1)$, the surrogate model exploits both approximations. The LFM part in (8) ensures that the algorithm will work if the coarse model is poor or even wrong.

The MCM $\boldsymbol{R}_m^{(i)}(\boldsymbol{x}_f)$ utilizes the linear frequency SM

$$\begin{aligned}\boldsymbol{R}_f(\boldsymbol{x}_f, \omega_j) &\approx \boldsymbol{R}_m^{(i)}(\boldsymbol{x}_f, \omega_j)\\ &= \boldsymbol{R}_c\left(\boldsymbol{P}^{(i)}(\boldsymbol{x}_f, \omega_j), P_\omega^{(i)}(\boldsymbol{x}_f, \omega_j)\right),\\ &\quad j = 1, 2, \ldots, N_\omega\end{aligned} \tag{9}$$

where

$$\begin{bmatrix}\boldsymbol{P}^{(i)}(\boldsymbol{x}_f, \omega_j)\\ P_\omega^{(i)}(\boldsymbol{x}_f, \omega_j)\end{bmatrix} = \begin{bmatrix}\boldsymbol{B}^{(i)} & \boldsymbol{s}^{(i)}\\ \boldsymbol{t}^{(i)T} & \sigma^{(i)}\end{bmatrix}\begin{bmatrix}\Delta\boldsymbol{x}_f\\ \omega_j\end{bmatrix} + \begin{bmatrix}\boldsymbol{c}^{(i)}\\ \gamma^{(i)}\end{bmatrix}. \tag{10}$$

The parameters $\boldsymbol{B}^{(i)} \in \Re^{n\times n}$, $\boldsymbol{s}^{(i)} \in \Re^{n\times 1}$, $\boldsymbol{t}^{(i)} \in \Re^{n\times 1}$, $\boldsymbol{c}^{(i)} \in \Re^{n\times 1}$, $\sigma^{(i)} \in \Re^{1\times 1}$, and $\gamma^{(i)} \in \Re^{1\times 1}$ are the mapping parameters. ω_j is the jth simulation frequency, $j = 1, 2, \ldots, N_\omega$. Here, a fine-model point $\boldsymbol{x}_f$ and frequency ω_j correspond to a coarse-model point $\boldsymbol{P}^{(i)}(\boldsymbol{x}_f, \omega_j)$ and coarse-model frequency $P_\omega^{(i)}(\boldsymbol{x}_f, \omega_j)$. Notice that (10) defaults to the frequency-insensitive mapping utilized by the ASM, TRASM, and HASM algorithms if $\boldsymbol{s}^{(i)} = \boldsymbol{t}^{(i)} = \boldsymbol{0}$, $\sigma^{(i)} = 1$, and $\gamma^{(i)} = 0$.

The advantage of utilizing (10) is illustrated by Fig. 1. It is required to extract the coarse point $\boldsymbol{x}_c$ corresponding to a given fine point $\boldsymbol{x}_f$. Previous SM-based algorithms utilize the PE procedure

$$\boldsymbol{x}_c = \arg\left\{\min_{\boldsymbol{x}_c} \|\boldsymbol{R}_f(\boldsymbol{x}_f) - \boldsymbol{R}_c(\boldsymbol{x}_c)\|\right\}. \tag{11}$$

Fig. 1(a) also shows the coarse-model response at the starting point for (11). The PE optimizer may not have enough information to align the almost disjoint responses. However, the responses align perfectly if a frequency transformation $\omega_c = P_\omega(\omega)$ is applied to the coarse-model frequency axis. This implies that the two models are simulated at different

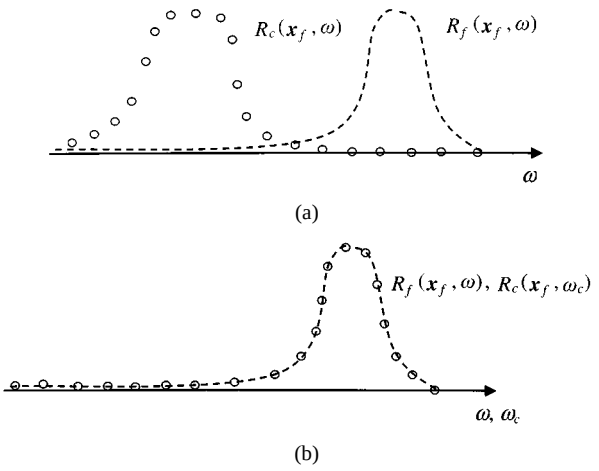

Fig. 1. Illustration of the frequency-sensitive mapping concept. (a) A significant frequency band shift exists between fine- and coarse-model responses at the initial iteration. (b) The coarse-model frequency is transformed such that both responses match.

frequencies. Fig. 1(b) shows the aligned responses. It follows that (10) allows another degree of freedom in aligning the coarse and fine models.

Utilizing a frequency sensitive mapping also enables indirect estimation of the fine-model derivatives. Using (9), the Jacobian of the mapped coarse-model responses $\boldsymbol{J}_m(\boldsymbol{x}_f^{(k)},\omega_j)\in\Re^{N_r\times n}$ at a point $\boldsymbol{x}_f^{(k)}$ and frequency ω_j is given by

$$\begin{aligned}\boldsymbol{J}_m\left(\boldsymbol{x}_f^{(k)},\omega_j\right)&=\left(\frac{\partial \boldsymbol{R}_m^T(\boldsymbol{x}_f,\omega)}{\partial \boldsymbol{x}_f}\right)^T\Bigg|_{\substack{\boldsymbol{x}_f=\boldsymbol{x}_f^{(k)}\\ \omega=\omega_j}}\\&=\left(\frac{\partial \boldsymbol{P}^T}{\partial \boldsymbol{x}_f}\,\frac{\partial \boldsymbol{R}_c^T(\boldsymbol{P},P_\omega)}{\partial \boldsymbol{P}}+\frac{\partial P_\omega}{\partial \boldsymbol{x}_f}\right.\\&\quad\left.\times\,\frac{\partial \boldsymbol{R}_c^T(\boldsymbol{P},P_\omega)}{\partial P_\omega}\right)^T\Bigg|_{\substack{\boldsymbol{P}=\boldsymbol{P}^{(i)}(\boldsymbol{x}_f^{(k)},\omega_j)\\ P_\omega=P_\omega^{(i)}(\boldsymbol{x}_f^{(k)},\omega_j)}}.\end{aligned}\tag{12}$$

For the case of the linear frequency-sensitive mapping (10), (12) becomes

$$\begin{aligned}\boldsymbol{J}_m\left(\boldsymbol{x}_f^{(k)},\omega_j\right)&=\left(\left(\frac{\partial \boldsymbol{R}_c^T(\boldsymbol{P},P_\omega)}{\partial \boldsymbol{P}}\right)^T\boldsymbol{B}^{(i)}\right.\\&\quad\left.+\,\frac{\partial \boldsymbol{R}_c(\boldsymbol{P},P_\omega)}{\partial P_\omega}\boldsymbol{t}^{(i)T}\right)\Bigg|_{\substack{\boldsymbol{P}=\boldsymbol{P}^{(i)}(\boldsymbol{x}_f^{(k)},\omega_j)\\ P_\omega=P_\omega^{(i)}(\boldsymbol{x}_f^{(k)},\omega_j)}}.\end{aligned}\tag{13}$$

Equation (13) utilizes only coarse-model derivatives in estimating the MCM derivatives. It defaults to the lemma utilized by the HASM algorithm [4]

$$\boldsymbol{J}_m\left(\boldsymbol{x}_f^{(k)},\omega_j\right)=\boldsymbol{J}_c\left(\boldsymbol{P}^{(i)}\left(\boldsymbol{x}_f^{(k)},\omega_j\right),P_\omega^{(i)}\left(\boldsymbol{x}_f^{(k)},\omega_j\right)\right)\boldsymbol{B}^{(i)}\tag{14}$$

for the case of a linear frequency-insensitive mapping $\boldsymbol{P}^{(i)}(\boldsymbol{x}_f,\omega)=\boldsymbol{B}^{(i)}\Delta\boldsymbol{x}_f+\boldsymbol{c}^{(i)}$ and $P_\omega^{(i)}(\boldsymbol{x}_f,\omega)=\omega$.

The MCM should approximate the fine model over a region of fine-model parameters and frequency. The mapping parameters are thus obtained through the optimization procedure

$$\begin{aligned}&\left[\boldsymbol{B}^{(i)},\boldsymbol{s}^{(i)},\boldsymbol{t}^{(i)},\sigma^{(i)},\boldsymbol{c}^{(i)},\gamma^{(i)}\right]\\&\quad=\arg\left\{\min_{\boldsymbol{B},\boldsymbol{s},\boldsymbol{t},\sigma,\boldsymbol{c},\gamma}\left\|\begin{bmatrix}\boldsymbol{e}_1 & \boldsymbol{e}_2 & \cdots & \boldsymbol{e}_{N_p}\end{bmatrix}^T\right\|\right\}\end{aligned}\tag{15}$$

$$\boldsymbol{e}_k=\boldsymbol{R}_m\left(\boldsymbol{x}_f^{(k)}\right)-\boldsymbol{R}_f\left(\boldsymbol{x}_f^{(k)}\right)\quad\forall\boldsymbol{x}_f^{(k)}\in V^{(i)}\tag{16}$$

where $V^{(i)}$ is a set of fine-model points whose cardinality is $|V^{(i)}|=N_p$. $V^{(i)}$ is constructed through an iterative process. Initially, we set $V^{(i)}=\{\boldsymbol{x}_f^{(i)}\}$. The two conditions

$$\begin{aligned}&\frac{\left(\boldsymbol{x}_f-\boldsymbol{x}_f^{(i)}\right)^T\left(\boldsymbol{x}_f^{(k)}-\boldsymbol{x}_f^{(i)}\right)}{\left\|\left(\boldsymbol{x}_f-\boldsymbol{x}_f^{(i)}\right)\right\|\left\|\boldsymbol{x}_f^{(k)}-\boldsymbol{x}_f^{(i)}\right\|}\le 1-\varepsilon\\&\qquad\forall\boldsymbol{x}_f^{(k)}\in V^{(i)}\quad\text{and}\quad 0<\left\|\boldsymbol{x}_f-\boldsymbol{x}_f^{(i)}\right\|<\alpha\end{aligned}\tag{17}$$

are checked $\forall\boldsymbol{x}_f\in S_f^{(i)}$, the set of simulated fine-model points up to the ith iteration. The first condition ensures better coverage by the points in $V^{(i)}$. The second condition rejects points outside an α neighborhood of $\boldsymbol{x}_f^{(i)}$. We denote α as the extraction radius. A point $\boldsymbol{x}_f$ is added to $V^{(i)}$ if (17) is satisfied.

If the $(i-1)$th iteration is unsuccessful, the MCM should be improved. This is important to guarantee a successful iteration in the ith iteration. However, no improvement is possible if (17) results in $V^{(i)}=V^{(i-1)}$. In this case, an additional perturbation $\Delta\boldsymbol{x}$ is generated by the algorithm. $\Delta\boldsymbol{x}$ is obtained by solving

$$\Delta\boldsymbol{x}=\arg\left\{\min_{\Delta\boldsymbol{x}\in S_v}\max_{\boldsymbol{x}_f^{(k)}\in V^{(i)}}\frac{\Delta\boldsymbol{x}^T\left(\boldsymbol{x}_f^{(k)}-\boldsymbol{x}_f^{(i)}\right)}{\|\Delta\boldsymbol{x}\|\left\|\boldsymbol{x}_f^{(k)}-\boldsymbol{x}_f^{(i)}\right\|}\right\}\tag{18}$$

where

$$S_v=\left\{\pm\alpha\,\frac{\boldsymbol{v}^{(i)}}{\left\|\boldsymbol{v}^{(i)}\right\|}\;\middle|\;\boldsymbol{J}_f^{(i)T}\boldsymbol{J}_f^{(i)}\boldsymbol{v}^{(i)}=\tau^{(i)}\boldsymbol{v}^{(i)}\text{ and }\tau^{(i)}>0\right\}.\tag{19}$$

The set S_v contains perturbations of length α in the direction of the eigenvectors of the matrix $\boldsymbol{J}_f^{(i)T}\boldsymbol{J}_f^{(i)}$. A similar approach is utilized by the aggressive parameter extraction (APE) [15] algorithm. These perturbations capture the functional behavior of the fine model within the considered region. $\Delta\boldsymbol{x}$ is a perturbation in S_v that maximizes the coverage of the α neighborhood. The point $\boldsymbol{x}_f^{(i)}+\Delta\boldsymbol{x}$ is then simulated and added to $V^{(i)}$. The construction of $V^{(i)}$ is illustrated in Fig. 2.

IV. Algorithm

The ith iteration of the algorithm proceeds as follows. First, the set $V^{(i)}$ is constructed. The mapping parameters are then estimated using the optimization procedure (15) and (16). The suggested step $\boldsymbol{h}^{(i)}$ is obtained by solving (7), where the surrogate model is given by (8). Notice that (7) utilizes only coarse-model simulations and can be solved using traditional optimization methods.

If the response $\boldsymbol{R}_c^*$ is good enough, we may be satisfied with a design for which $\boldsymbol{R}_f(\boldsymbol{x}_f)\approx\boldsymbol{R}_c^*$. In this case, we select U as

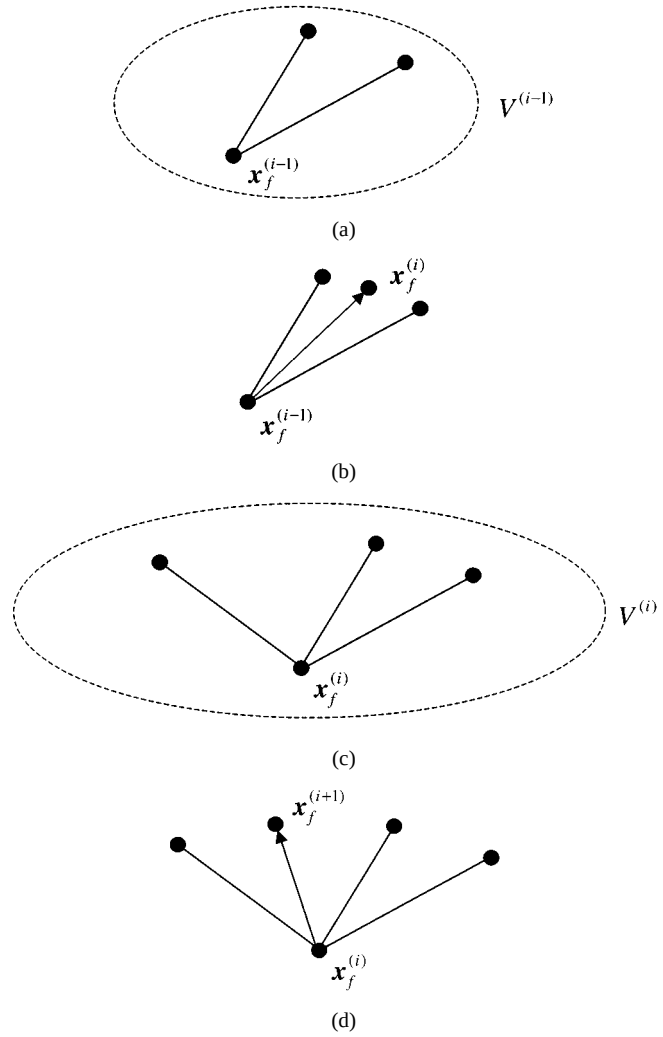

Fig. 2. Illustration of the selection of the PE points. (a) At the $(i-1)$th iteration, we have the point $\boldsymbol{x}_f^{(i-1)}$ and the set $V^{(i-1)}$. (b) A new point is generated by the algorithm that does not satisfy the success criterion. (c) $\boldsymbol{x}_f^{(i-1)}$ becomes $\boldsymbol{x}_f^{(i)}$, the previous perturbation $\boldsymbol{h}^{(i)}$ is excluded from $V^{(i)}$, and the algorithm generates an alternative perturbation. (d) The set $V^{(i)}$ is used to extract new mapping parameters and predict a successful iterate.

$||\boldsymbol{R}_f(\boldsymbol{x}_f) - \boldsymbol{R}_c^*||$. However, if the optimality of the design is the main concern, U may be selected as the generalized minimax objective function [13].

The optimizer utilized in solving (7) may require first-order derivatives in addition to the surrogate model responses. The surrogate model Jacobian $\boldsymbol{J}_s(\boldsymbol{x}_f^{(i)}) \in \Re^{m\times n}$ is given by

$$\boldsymbol{J}_s\left(\boldsymbol{x}_f^{(i)}\right) = \lambda^{(i)}\boldsymbol{J}_m\left(\boldsymbol{x}_f^{(i)}\right) + \left(1-\lambda^{(i)}\right)\boldsymbol{J}_f\left(\boldsymbol{x}_f^{(i)}\right). \quad (20)$$

$\boldsymbol{J}_m(\boldsymbol{x}_f^{(i)}) \in \Re^{m\times n}$ is the Jacobian of the mapped coarse-model responses at all frequencies. Using (13), it is given by (21), shown at the bottom of the page.

The step $\boldsymbol{h}^{(i)}$ obtained through (7) is accepted if it improves the fine-model objective function. Otherwise, it is rejected. The parameters $\boldsymbol{J}_f^{(i)}$, $\delta^{(i)}$, and $\lambda^{(i)}$ are updated in every iteration. Broyden's formula [14] is used to update $\boldsymbol{J}_f^{(i)}$. Initially, we set $\boldsymbol{J}_f^{(1)} = \boldsymbol{J}_c^*$, the Jacobian of the coarse-model response at $\boldsymbol{x}_c^*$. The trust region size $\delta^{(i)}$ is updated based on the ratio between the actual reduction r_a in U and the predicted reduction r_p. The ratio

$$\rho = \frac{r_a}{r_p} = \frac{U\left(\boldsymbol{R}_f\left(\boldsymbol{x}_f^{(i)}\right)\right) - U\left(\boldsymbol{R}_f\left(\boldsymbol{x}_f^{(i)}+\boldsymbol{h}^{(i)}\right)\right)}{U\left(\boldsymbol{R}_s^{(i)}\left(\boldsymbol{x}_f^{(i)}\right)\right) - U\left(\boldsymbol{R}_s^{(i)}\left(\boldsymbol{x}_f^{(i)}+\boldsymbol{h}^{(i)}\right)\right)} \quad (22)$$

is thus evaluated at the end of each iteration. If $\rho \geq 0.75$, the surrogate model has good accuracy and we set $\delta^{(i+1)} = \pi_1\delta^{(i)}$, $\pi_1 > 1.0$. If $\rho \leq 0.10$, we set $\delta^{(i+1)} = \pi_2\delta^{(i)}$, $0 < \pi_2 < 1.0$. Otherwise, we set $\delta^{(i+1)} = \delta^{(i)}$. $\lambda^{(i)}$ is updated to favor the more accurate model, either the LFM or the MCM. It is initialized by $\lambda^{(1)} = 1$. The utilized update is

$$\lambda^{(i+1)} = \frac{\left\|\boldsymbol{E}_l^{(i)}\right\|}{\left\|\boldsymbol{E}_l^{(i)}\right\| + \left\|\boldsymbol{E}_m^{(i)}\right\|} \quad (23)$$

if $||\boldsymbol{E}_l^{(i)}|| \leq \varepsilon_\ell$. Otherwise, we set $\lambda^{(i+1)} = 1$. The vectors $\boldsymbol{E}_m^{(i)} = \boldsymbol{R}_m^{(i)}(\boldsymbol{x}_f^{(i)} + \boldsymbol{h}^{(i)}) - \boldsymbol{R}_f(\boldsymbol{x}_f^{(i)} + \boldsymbol{h}^{(i)})$ and $\boldsymbol{E}_l^{(i)} = \boldsymbol{R}_f(\boldsymbol{x}_f^{(i)}) + \boldsymbol{J}_f^{(i)}\boldsymbol{h}^{(i)} - \boldsymbol{R}_f(\boldsymbol{x}_f^{(i)} + \boldsymbol{h}^{(i)})$ define the prediction error using the MCM and LFM, respectively. The update (23) assigns higher weight to the more accurate model. It should be noted that the LFM starts with low accuracy. However, Broyden's update iteratively improves the accuracy of this model. Our algorithm terminates if $n+1$ consecutive unsuccessful iterations are carried out or if $||\boldsymbol{h}^{(i)}||$ becomes sufficiently small. Fig. 3 illustrates one iteration of the algorithm.

The algorithm can be summarized by the following steps.

- Step 1) Given $\boldsymbol{x}_f^{(1)} = \boldsymbol{x}_c^*$, $\lambda^{(1)} = 1$, $\delta^{(1)}$, α, $\boldsymbol{J}_f^{(1)} = \boldsymbol{J}_c^*$, and $i = 1$.
- Step 2) Construct $V^{(i)}$.
- Step 3) Apply the optimization procedure (15) and (16) to obtain the mapping parameters.
- Step 4) Obtain the suggested step $\boldsymbol{h}^{(i)}$ by solving (7).
- Step 5) If $U(\boldsymbol{R}_f(\boldsymbol{x}_f^{(i)}+\boldsymbol{h}^{(i)})) < U(\boldsymbol{R}_f(\boldsymbol{x}_f^{(i)}))$, set $\boldsymbol{x}_f^{(i+1)} = \boldsymbol{x}_f^{(i)} + \boldsymbol{h}^{(i)}$ else $\boldsymbol{x}_f^{(i+1)} = \boldsymbol{x}_f^{(i)}$.
- Step 6) Update $\boldsymbol{J}_f^{(i)}$, $\delta^{(i)}$ and $\lambda^{(i)}$.
- Step 7) If the stopping criterion is satisfied stop.
- Step 8) Set $i = i+1$ and go to Step 2.

A flowchart of the algorithm is shown in Fig. 4.

V. Examples

A. Capacitively Loaded 10 : 1 Impedance Transformer

We consider the design of a capacitively loaded 10 : 1 impedance transformer [10]. The proposed fine and coarse models are shown in Figs. 5 and 6, respectively. The values

$$\boldsymbol{J}_m\left(\boldsymbol{x}_f^{(i)}\right) = \left[\boldsymbol{J}_m^T\left(\boldsymbol{x}_f^{(i)},\omega_1\right) \quad \boldsymbol{J}_m^T\left(\boldsymbol{x}_f^{(i)},\omega_2\right) \quad \cdots \quad \boldsymbol{J}_m^T\left(\boldsymbol{x}_f^{(i)},\omega_{N_\omega}\right)\right]^T \quad (21)$$

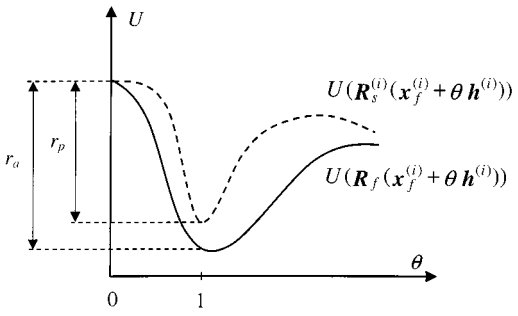

Fig. 3. Illustration of the ith iteration of the algorithm.

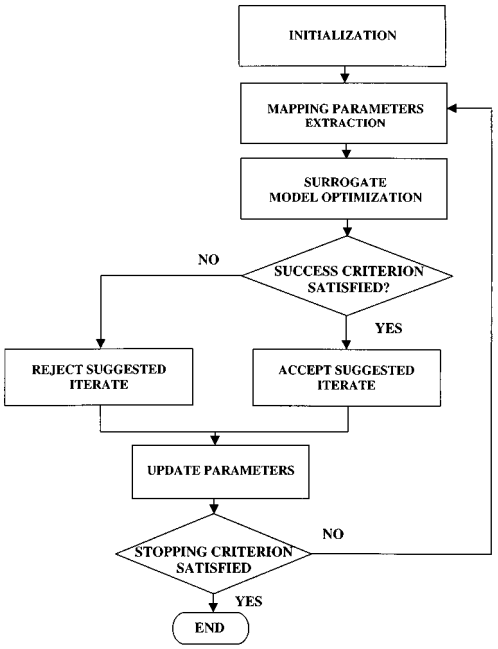

Fig. 4. Flowchart of the algorithm.

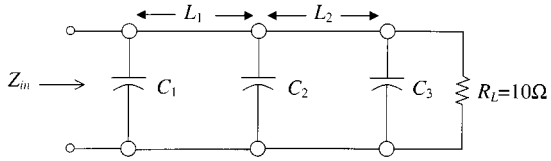

Fig. 5. Fine model of the capacitively loaded 10 : 1 impedance transformer.

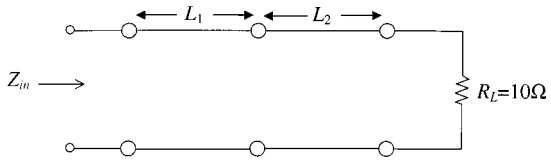

Fig. 6. Coarse model of the capacitively loaded 10 : 1 impedance transformer.

of the capacitances that we use are given in Table I. Design specifications are

$$|S_{11}| \le 0.50, \qquad \text{for } 0.5 \text{ GHz} \le \omega \le 1.5 \text{ GHz}. \tag{24}$$

The electrical lengths of the two transmission lines at 1.0 GHz are selected as designable parameters. The characteristic impedances are kept fixed at the optimal values given in Table II. Both

TABLE I
FINE-MODEL CAPACITANCES FOR THE CAPACITIVELY LOADED IMPEDANCE TRANSFORMER

Capacitance	Value
C_1	10
C_2	10
C_3	10
all values are in pF	

TABLE II
CHARACTERISTIC IMPEDANCES FOR THE CAPACITIVELY LOADED IMPEDANCE TRANSFORMER

Impedance	Value
Z_1	2.23615
Z_2	4.47230
all values are in ohm	

TABLE III
INITIAL AND FINAL DESIGNS FOR THE CAPACITIVELY LOADED IMPEDANCE TRANSFORMER

Parameter	$\boldsymbol{x}_f^{(1)}$	$\boldsymbol{x}_f^{(6)}$
L_1	90.0000	81.59880
L_2	90.0000	74.38324
all values are in degrees		

models make use of the ideal transmission-line model available in OSA90/hope.[1] Eleven frequency points are simulated per sweep. We utilized the real and imaginary parts of S_{11} in the optimization procedure (15) and (16). The initial trust region size and extraction radius are $\delta^{(1)} = 0.09\|\boldsymbol{x}_c^*\|_\infty$ and $\alpha = 0.09\|\boldsymbol{x}_c^*\|_\infty$, respectively. The algorithm executed five iterations. Only the first two are successful. The total number of fine-model simulations is seven. The initial and final designs are given in Table III. The corresponding responses are shown in Figs. 7 and 8, respectively. The final mapping is given by

$$\begin{aligned}
\boldsymbol{B}^{(6)} &= \begin{bmatrix} 1.12886 & 0.19245 \\ -0.17669 & 1.19167 \end{bmatrix} \\
\boldsymbol{c}^{(6)} &= \begin{bmatrix} 84.52643 \\ 87.95123 \end{bmatrix} \\
\boldsymbol{s}^{(6)} &= \begin{bmatrix} -0.06863 \\ 0.06035 \end{bmatrix} \\
\boldsymbol{t}^{(6)} &= \begin{bmatrix} -0.00026 \\ -0.00212 \end{bmatrix} \\
\sigma^{(6)} &= 1.03243 \\
\gamma^{(6)} &= 0.00983.
\end{aligned} \tag{25}$$

The value of U in every iteration is shown in Fig. 9.

B. DFS Filter

The DFS fine model utilizes Sonnet's ***em***[2] through Empipe (see Fig. 10). The coarse model, shown in Fig. 11, exploits

[1]OSA90/hope and Empipe, version 4.0, Optimization Systems Associates Inc., Dundas, ON, Canada (now Agilent Technologies, Santa Rosa, CA), 1997.

[2]Sonnet Software Inc., Liverpool, NY, 1997.

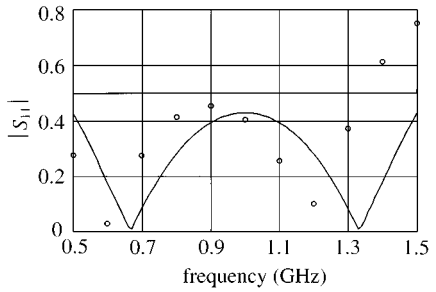

Fig. 7. Optimal coarse-model response (—) and the fine-model response (∘) at the starting point for the capacitively loaded 10 : 1 impedance transformer.

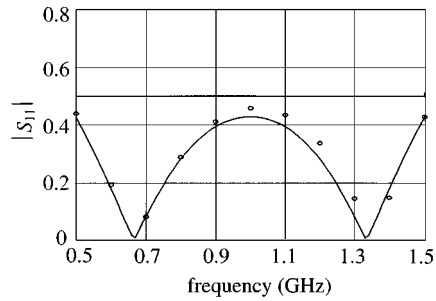

Fig. 8. Optimal coarse-model response (—) and the fine-model response (∘) at the final design for the capacitively loaded 10 : 1 impedance transformer.

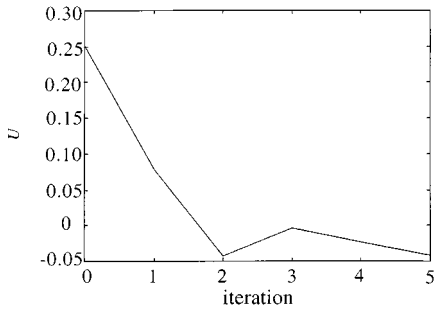

Fig. 9. Value of U in each iteration for the 10 : 1 impedance transformer.

the microstrip line and microstrip T-junction models available in OSA90/hope. The coupling between the folded stubs and microstrip line is simulated using equivalent capacitors. The values of these capacitors are determined using Walker's formulas [16]. Jansen's microstrip bend model [17] is used to model the folding effect of the stub.

The design specifications are

$$|S_{21}| \geq -3 \text{ dB}, \qquad \text{for } \omega \leq 9.5 \text{ GHz and } 16.5 \text{ GHz} \leq \omega$$
$$|S_{21}| \leq -30 \text{ dB}, \qquad \text{for } 12 \text{ GHz} \leq \omega \leq 14 \text{ GHz}. \tag{26}$$

L_1, L_2, and S are selected as designable parameters. W_1 and W_2 are fixed at 4.8 mil. Only 11 frequency points are utilized per sweep. The mapping parameters are obtained using the real and imaginary parts of S_{21}. The initial trust region size and extraction radius are $\delta^{(1)} = 0.09||\boldsymbol{x}_c^*||_\infty$ and $\alpha = 0.09||\boldsymbol{x}_c^*||_\infty$. The width S is scaled by a factor of 6.0 to make the problem better conditioned.

The design procedure is carried out with the interpolation option of Empipe disabled. Here, every iterate is snapped to the nearest on-grid point. Our algorithm carried out only 16 iterations. A total of 18 calls to Empipe (18 ***em*** simulations) were needed. The initial and final designs are given in Table IV. The corresponding responses are shown in Figs. 12 and 13. The

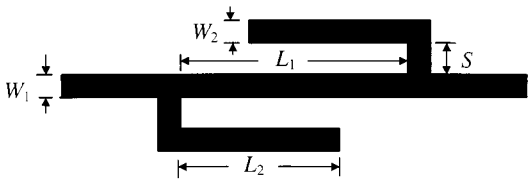

Fig. 10. DFS filter.

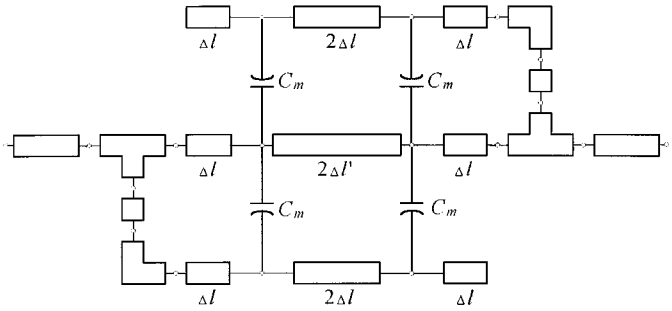

Fig. 11. Coarse model of the DFS filter.

TABLE IV
INITIAL AND FINAL DESIGNS FOR THE DFS FILTER

Parameter	$\boldsymbol{x}_f^{(1)}$	$\boldsymbol{x}_f^{(17)}$
S	9.60	6.4
L_2	60.80	84.8
L_1	67.2	86.4
all values are in mil		

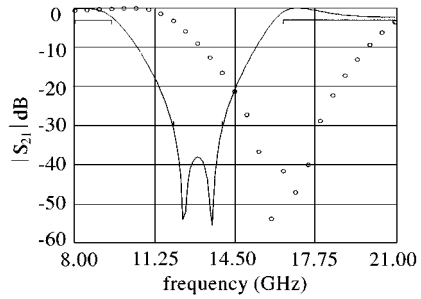

Fig. 12. Optimal coarse-model response (—) and the fine-model response (∘) at the starting design for the DFS filter.

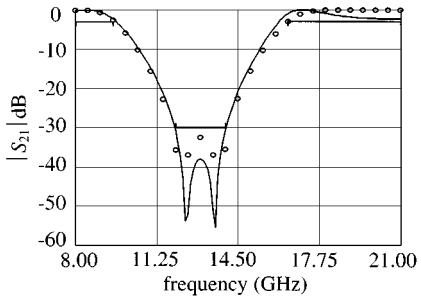

Fig. 13. Optimal coarse-model response (—) and the fine-model response (∘) at the final design for the DFS filter.

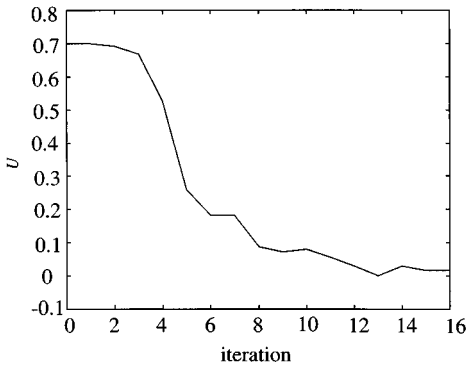

Fig. 14. Value of U at every iteration for the DFS filter.

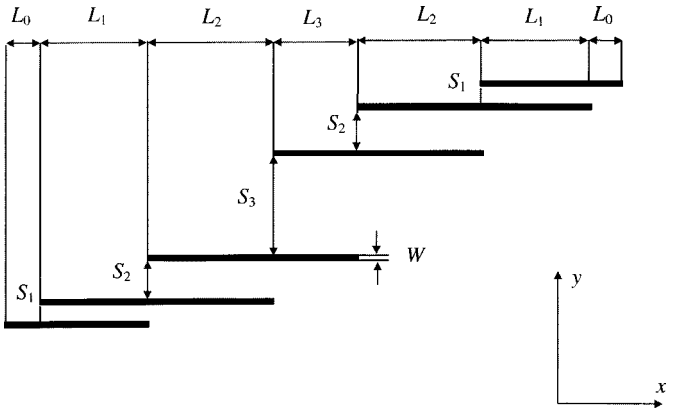

Fig. 15. HTS filter.

value of U in each iteration is shown in Fig. 14. The final mapping parameters are

$$\boldsymbol{B}^{(17)} = \begin{bmatrix} 1.03074 & 0.11174 & 0.00031 \\ -0.20595 & 0.96384 & 0.00365 \\ -0.35144 & 0.34204 & 0.78257 \end{bmatrix}$$

$$\boldsymbol{c}^{(17)} = \begin{bmatrix} 236.1134 \\ 21.5218 \\ 74.8218 \end{bmatrix}$$

$$\boldsymbol{s}^{(17)} = \begin{bmatrix} 0.44639 \\ 0.70939 \\ 0.50045 \end{bmatrix}$$

$$\boldsymbol{t}^{(17)} = \begin{bmatrix} 0.03854 \\ -0.01167 \\ 0.00439 \end{bmatrix}$$

$$\sigma^{(17)} = 1.13771$$

$$\gamma^{(17)} = -0.55168. \tag{27}$$

C. HTS Filter

We also consider the design of an HTS filter [12]. This filter is shown in Fig. 15. The design specifications are

$$\begin{aligned} &|S_{21}| \le 0.05, && \text{for } \omega \le 3.967 \text{ GHz and } 4.099 \text{ GHz} \le \omega \\ &|S_{21}| \ge 0.95, && \text{for } 4.008 \text{ GHz} \le \omega \le 4.058 \text{ GHz}. \end{aligned} \tag{28}$$

The designable parameters are L_1, L_2, L_3, S_1, S_2, and S_3. We take $L_0 = 50$ mil and $W = 7$ mil. The coarse model exploits the empirical models of microstrip lines, coupled lines, and open stubs available in OSA90/hope (see Fig. 16). The fine model employs Sonnet's ***em*** through Empipe. We utilized the real and imaginary parts of both S_{11} and S_{21} in the optimization procedure (15) and (16). The initial trust region size is $\delta^{(1)} = 0.20\|\boldsymbol{x}_c^*\|_\infty$. The α neighborhood is selected as an n-dimensional box. This takes into account that the response is more sensitive to the lengths than the widths. The interpolation option of Empipe is disabled to make the optimization time reasonable.

Here, we fix $\boldsymbol{s}^{(i)} = \boldsymbol{t}^{(i)} = \boldsymbol{0}$. The rest of the mapping parameters are obtained using (15) and (16). This implies that the frequency and SMs are decoupled. This approach reduces the number of optimizable parameters in (15) and (16). Consequently, it makes the extraction of the mapping parameters better conditioned. This approach is motivated by the fact that previous examples have effectively decoupled mappings ($\boldsymbol{s}^{(i)} \approx \boldsymbol{0}$ and $\boldsymbol{t}^{(i)} \approx \boldsymbol{0}$).

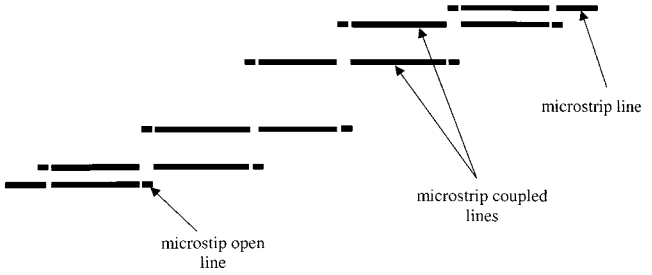

Fig. 16. Coarse model of the HTS filter.

TABLE V
MATERIAL AND PHYSICAL PARAMETERS FOR THE HTS FILTER

Model Parameter	OSA90/hope	*em*
substrate dielectric constant	23.425	23.425
substrate thickness (mil)	19.9516	19.9516
shielding cover height (mil)	∞	250
Conducting material thickness	0	0
Substrate dielectric loss tangent	0	0
Resistivity of metal (Ωm)	0	0
Surface roughness of metal	0	—
Magnetic loss tangent	—	0
Surface reactance (Ω/sq)	—	0
x-grid cell size (mil)	—	1.00
y-grid cell size (mil)	—	1.75

TABLE VI
INITIAL AND FINAL DESIGNS FOR THE HTS FILTER

Parameter	$\boldsymbol{x}_f^{(1)}$	$\boldsymbol{x}_f^{(8)}$
L_1	188.00	188.00
L_2	198.00	192.00
L_3	189.00	187.00
S_1	22.75	22.75
S_2	99.75	78.75
S_3	112.00	91.00
all values are in mils		

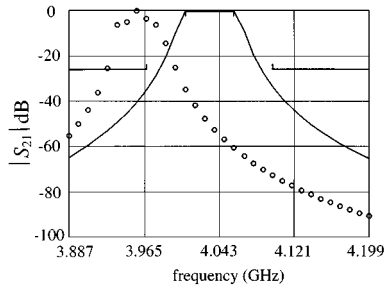

Fig. 17. Optimal coarse-model response (—) and the fine-model response (∘) at the initial design for the HTS filter.

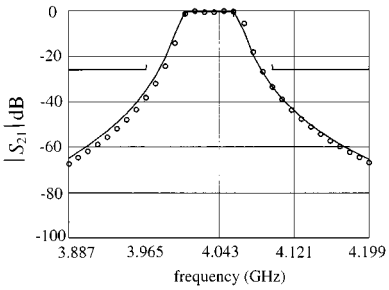

Fig. 18. Optimal coarse-model response (—) and the fine-model response (∘) at the final design for the HTS filter.

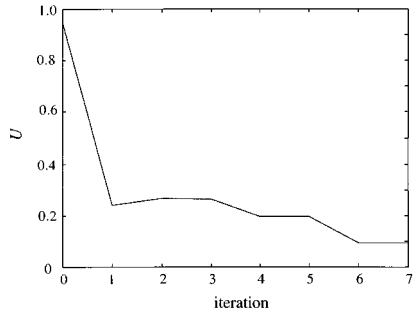

Fig. 19. Value of U at every iteration for the HTS filter.

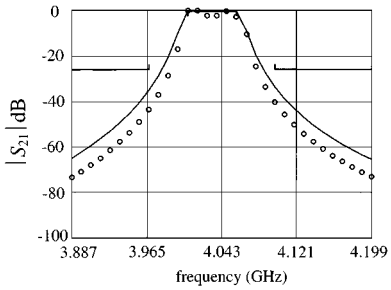

Fig. 20. Optimal coarse-model response (—) and the fine-model response (∘) at the end of the first iteration for the HTS filter.

The HTS design is carried out assuming lossless substrate dielectric. A relatively coarse grid size is used. The material and physical parameters values used in both OSA90/hope and ***em*** are shown in Table V. The fine model is simulated at 16 frequency points per sweep. Starting from the snapped optimal coarse design, the final design is reached in seven iterations only. A total of seven fine-model simulations are used. The initial and final designs are given in Table VI. The corresponding responses are shown in Figs. 17 and 18, respectively. The value of U in each iteration is shown in Fig. 19.

Fig. 20 illustrates the fine-model response at the end of the first iteration. It is seen that the fine-model response is well aligned in the proper band using only one fine-model simulation. This illustrates the power of the algorithm in handling significant frequency shifts. The final mapping is given by (29), shown at the bottom of the page.

VI. Conclusion

In this paper, we have presented a breakthrough algorithm for efficient optimization of microwave circuits. The algorithm integrates, for the first time, SM optimization with surrogate model optimization. It exploits a surrogate model in the form of a convex combination of an MCM and LFM. The MCM utilizes a novel frequency SM. During optimization, the coarse and fine models are simulated over different frequency ranges. This approach is shown to be powerful, especially if significant response shift exists. It also enables indirect estimation of the derivatives of fine-model responses. The algorithm is suc-

$$\boldsymbol{B}^{(8)} = \begin{bmatrix} 1.08894 & 0.00855 & -0.01082 & 0.01422 & -0.07505 & -0.00979 \\ -0.00481 & 0.96627 & -0.00695 & 0.00912 & -0.03234 & -0.00592 \\ 0.00828 & -0.00831 & 0.97551 & -0.01433 & 0.02963 & 0.00955 \\ -0.01513 & 0.01509 & -0.02016 & 1.04437 & 0.01671 & -0.01747 \\ -0.01324 & 0.01320 & -0.01766 & 0.02317 & 1.03175 & -0.01541 \\ -0.01401 & 0.01400 & -0.01869 & 0.02453 & 0.00672 & 0.95969 \end{bmatrix}$$

$$\boldsymbol{c}^{(8)} = \begin{bmatrix} 180.61046 \\ 190.38887 \\ 180.53859 \\ 23.96889 \\ 98.89007 \\ 113.32096 \end{bmatrix}$$

$$\boldsymbol{t}^{(8)} = \boldsymbol{s}^{(8)} = \boldsymbol{0}$$

$$\sigma^{(8)} = 1.07264$$

$$\gamma^{(8)} = -0.12873 \tag{29}$$

cessfully illustrated through the design of microwave filters and transformers.

REFERENCES

[1] M. H. Bakr, J. W. Bandler, K. Madsen, J. E. Rayas-Sánchez, and J. Søndergaard, "Space mapping optimization of microwave circuits exploiting surrogate models," in *IEEE MTT-S Int. Microwave Symp. Dig.*, Boston, MA, 2000, pp. 1785–1788.

[2] J. W. Bandler, R. M. Biernacki, S. H. Chen, R. H. Hemmers, and K. Madsen, "Electromagnetic optimization exploiting aggressive space mapping," *IEEE Trans. Microwave Theory Tech.*, vol. 43, pp. 2874–2882, Dec. 1995.

[3] M. H. Bakr, J. W. Bandler, R. M. Biernacki, S. H. Chen, and K. Madsen, "A trust region aggressive space mapping algorithm for EM optimization," *IEEE Trans. Microwave Theory Tech.*, vol. 46, pp. 2412–2425, Dec. 1998.

[4] M. H. Bakr, J. W. Bandler, N. Georgieva, and K. Madsen, "A hybrid aggressive space mapping algorithm for EM optimization," *IEEE Trans. Microwave Theory Tech.*, vol. 47, pp. 2440–2449, Dec. 1999.

[5] A. J. Booker, J. E. Dennis, Jr., P. D. Frank, D. B. Serafini, V. Torczon, and M. W. Trosset, "A rigorous framework for optimization of expensive functions by surrogates," *Structural Optimization*, vol. 17, pp. 1–13, 1999.

[6] V. Torczon and M. W. Trosset, "Using Approximations to Accelerate Engineering Design Optimization," ICASE, Langley Res. Center, Hampton, VA, Tech. Rep. 98-33, 1998.

[7] N. Alexandrov, J. E. Dennis, Jr., R. M. Lewis, and V. Torczon, "A trust region framework for managing the use of approximation models in optimization," *Structural Optimization*, vol. 15, pp. 16–23, 1998.

[8] J. W. Bandler, M. A. Ismail, J. E. Rayas-Sánchez, and Q. J. Zhang, "Neuromodeling of microwave circuits exploiting space mapping technology," *IEEE Trans. Microwave Theory Tech.*, vol. 47, pp. 2417–2427, Dec. 1999.

[9] J. W. Bandler, N. Georgieva, M. A. Ismail, J. E. Rayas-Sánchez, and Q. J. Zhang, "A generalized space mapping tableau approach to device modeling," in *29th European Microwave Conf.*, vol. 3, Munich, Germany, 1999, pp. 231–234.

[10] J. W. Bandler, "Optimization methods for computer-aided design," *IEEE Trans. Microwave Theory Tech.*, vol. MTT-17, pp. 533–552, Aug. 1969.

[11] J. C. Rautio, private communication, 1992.

[12] J. W. Bandler, R. M. Biernacki, S. H. Chen, W. J. Gestinger, P. A. Grobelny, C. Moskowitz, and S. H. Talisa, "Electromagnetic design of high-temperature superconducting filters," *Int. J. Microwave Millimeter-Wave Computer-Aided Eng.*, vol. 5, pp. 331–343, 1995.

[13] J. W. Bandler, W. Kellermann, and K. Madsen, "A superlinearly convergent minimax algorithm for microwave circuit design," *IEEE Trans. Microwave Theory Tech.*, vol. MTT-33, pp. 1519–1530, Dec. 1985.

[14] C. G. Broyden, "A class of methods for solving nonlinear simultaneous equations," *Math. Comput.*, vol. 19, pp. 577–593, 1965.

[15] M. H. Bakr, J. W. Bandler, and N. Georgieva, "An aggressive approach to parameter extraction," *IEEE Trans. Microwave Theory Tech.*, vol. 47, pp. 2428–2439, Dec. 1999.

[16] C. S. Walker, *Capacitance, Inductance and Crosstalk Analysis*. Norwood, MA: Artech House, 1990.

[17] M. Kirschning, R. Jansen, and N. Koster, "Measurement and computer-aided modeling of microstrip discontinuities by an improved resonator method," in *IEEE MTT-S Int. Microwave Symp. Dig.*, Boston, MA, 1983, pp. 495–497.

Mohamed H. Bakr (S'98) was born in November 7, 1969. He received the B.Sc. degree (with distinction) in electronics and communications engineering and the M.Sc. degree in engineering mathematics from Cairo University, Cairo, Egypt, in 1992 and 1996, respectively, and the Ph.D. degree in electrical and computer engineering from McMaster University, Hamilton, ON, Canada, in 2000.

In October 1992, he joined the Department of Engineering Mathematics and Physics, Faculty of Engineering, Cairo University. In September 1996, he joined the Department of Electrical and Computer Engineering, McMaster University, where his research is carried out in the Simulation Optimization Systems Research Laboratory. He held the position of a student intern at Optimization Systems Associates Inc. from July 1997 to June 1998. He is currently a Post-Doctoral Fellow in the Department of Electrical and Computer Engineering, McMaster University. He is interested in optimization methods, computer-aided design, and modeling of microwave circuits and in neural-networks applications.

Mr. Bakr has held the Ontario Graduate Scholarship (OGS) for two consecutive years. He was also awarded a Natural Sciences and Engineering Research Council of Canada (NSERC) Post-Doctoral Fellowship in April 2000.

John W. Bandler (S'66–M'66–SM'74–F'78) was born in Jerusalem, on November 9, 1941. He studied at the Imperial College of Science and Technology, London, U.K., from 1960 to 1966. He received the B.Sc. (Eng.), Ph.D., and D.Sc. (Eng.) degrees from the University of London, London, U.K., in 1963, 1967, and 1976, respectively.

In 1966, he joined Mullard Research Laboratories, Redhill, Surrey, U.K. From 1967 to 1969, he was a Post-Doctorate Fellow and Sessional Lecturer at the University of Manitoba, Winnipeg, MB, Canada. In 1969, he joined McMaster University, Hamilton, ON, Canada, where he has served as Chairman of the Department of Electrical Engineering and Dean of the Faculty of Engineering. He is currently a Professor Emeritus in Electrical and Computer Engineering, and directs research in the Simulation Optimization Systems Research Laboratory. He is a member of the Micronet Network of Centres of Excellence. He was President of Optimization Systems Associates Inc. (OSA), which he founded in 1983, until November 20, 1997, the date of acquisition of OSA by Hewlett-Packard Company (HP). OSA implemented a first-generation yield-driven microwave computer-aided design (CAD) capability for Raytheon in 1985, followed by further innovations in linear and nonlinear microwave CAD technology for the Raytheon/Texas Instruments Incorporated Joint Venture MIMIC Program. OSA introduced the computer-aided engineering (CAE) systems RoMPE in 1988, HarPE in 1989, OSA90 and OSA90/hope in 1991, Empipe in 1992, and Empipe3D and EmpipeExpress in 1996. OSA created the product ***empath*** in 1996, which was marketed by Sonnet Software Inc., Liverpool, NY. He is President of the Bandler Corporation, Dundas, ON, Canada, which he founded in 1997. He has authored or co–authored over 320 papers from 1965 to 2000. He contributed to *Modern Filter Theory and Design* (New York: Wiley, 1973) and to *Analog Methods for Computer-aided Analysis and Diagnosis* (New York: Marcel Dekker, 1988). Four of his papers have been reprinted in *Computer-Aided Filter Design* (New York: IEEE Press, 1973), one in each of *Microwave Integrated Circuits* (Norwood, MA: Artech House, 1975), *Low-Noise Microwave Transistors and Amplifiers* (New York: IEEE Press, 1981), *Microwave Integrated Circuits, 2nd ed.* (Norwood, MA: Artech House, 1985), *Statistical Design of Integrated Circuits* (New York: IEEE Press, 1987), and *Analog Fault Diagnosis* (New York: IEEE Press, 1987). He joined the Editorial Boards of the *International Journal of Numerical Modeling* in 1987, the *International Journal of Microwave and Millimeterwave Computer-Aided Engineering* in 1989, and *Optimization and Engineering* in 1998. He was guest editor of the *International Journal of Microwave and Millimeter-Wave Computer-Aided Engineering* "Special Issue on Optimization-Oriented Microwave CAD" (1997).

Dr. Bandler is a Fellow of the Royal Society of Canada, a Fellow of the Institution of Electrical Engineers (IEE), U.K., a Fellow of the Engineering Institute of Canada, a member of the Association of Professional Engineers of the Province of Ontario (Canada), and a member of the Massachusetts Institute of Technology (MIT) Electromagnetics Academy. He was an associate editor of the IEEE TRANSACTIONS ON MICROWAVE THEORY AND TECHNIQUES (1969–1974), and has continued serving as a member of the Editorial Board. He was guest editor of the Special Issue on "Computer-Oriented Microwave Practices" of the IEEE TRANSACTIONS ON MICROWAVE THEORY AND TECHNIQUES (1974), guest co-editor of the Special Issue on "Process-Oriented Microwave CAD and Modeling" of the IEEE TRANSACTIONS ON MICROWAVE THEORY AND TECHNIQUES (1992), and guest editor of the Special Issue on "Automated Circuit Design Using Electromagnetic Simulators" of the TRANSACTIONS ON MICROWAVE THEORY AND TECHNIQUES (1997). He is currently co-chair of the MTT-1 Technical Committee on Computer-Aided Design. He was the recipient of the 1994 Automatic Radio Frequency Techniques Group (ARFTG) Automated Measurements Career Award.

Kaj Madsen was born in Denmark, in 1943. He received the Cand.Scient. degree in mathematics from the University of Aarhus, Aarhus, Denmark, in 1968, and the Dr.Techn. degree from the Technical University of Denmark, Lyngby, Denmark, in 1986.

From 1968 to 1988, he was a Lecturer in numerical analysis, apart from the 1973–1974 academic year, when he was with AERE Harwell, Didcot, U.K. Most of his career has been spent with the Institute for Numerical Analysis, Technical University of Denmark, but from 1981 to 1983, he was with the Computer Science Department, Copenhagen University. During the summer of 1978, he visited McMaster University, Hamilton, ON, Canada. In 1988, he became a Professor at the Institute for Numerical Analysis, Technical University of Denmark. In 1993, he joined the Department of Mathematical Modeling, Technical University of Denmark. From 1988 to 1993, and since 1995, he has been Head of this same department. His fields of interest in teaching and research are parallel algorithms, optimization, and interval analysis.

José Ernesto Rayas-Sánchez (S'88–M'89–SM'95) was born in Guadalajara, Jalisco, Mexico, on December 27, 1961. He received the B.Sc. degree in electronics engineering from the Instituto Tecnológico y de Estudios Superiores de Occidente (ITESO), Guadalajara, Mexico, in 1984, the Masters degree in electrical engineering at the Instituto Tecnológico y de Estudios Superiores de Monterrey (ITESM), Monterrey, Mexico, in 1989, and is currently working toward the Ph.D. degree in electrical engineering at McMaster University, Hamilton, ON, Canada.

From 1989 to 1997, he was a Full-Time Professor in the Electrical and Computer Engineering Department, ITESO. He joined the Simulation Optimization Systems Research Laboratory, McMaster University, in 1997. His research focuses on the development of novel methods and techniques for computer-aided modeling, design, and optimization of analog wireless electronic circuits and devices exploiting SM and ANNs.

Mr. Rayas-Sánchez was the recipient of a 1997–2000 Consejo Nacional de Ciencia y Tecnología (CONACYT) Scholarship presented by the Mexican Government, as well as a 2000–2001 Ontario Graduate Scholarship presented by the Ministry of Training for Colleges and Universities in Ontario.

Jacob Søndergaard, was born in Denmark, in 1975. He received the Cand.Polyt. degree from the Technical University of Denmark, Lyngby, Denmark, in 1999, and is currently working toward the Ph.D. degree in mathematical modeling at the Technical University of Denmark.

His fields of interest are in linear and nonlinear optimization.